Formation of Secondary Containment Systems Using Permeation of Colloidal Silica

John McCartney, Ph.D., P.E., M.ASCE[1]; Christianne L. Nogueira, D.Sc.[2]; Daniel Homes[3]; and Jorge G. Zornberg, Ph.D., P.E., M.ASCE[4]

Abstract: U.S. Environmental Protection Agency (USEPA) regulations require the capture of spills from liquid tanks containing hazardous chemicals by using a secondary containment system. Compacted clay or geomembrane liners are commonly used in secondary containment systems, but they are cumbersome when used in conjunction with existing liquid tanks because of pipeline networks surrounding the tanks. This study evaluates the formation of hydraulic barriers for secondary containment through the permeation of colloidal silica grout. A simplified infiltration model is presented to predict the downward movement of the colloidal silica grout into a soil layer, considering the time-dependent increase in dynamic viscosity of the colloidal silica for different concentrations of an electrolyte accelerator. Because the simplified infiltration model cannot predict the soil-grout interaction or the permeation of the colloidal silica by fingering, its results were calibrated by using the observations from a large-scale column test involving the permeation of colloidal silica into sand. The predicted position of the wetting front was found to match that of the experiment when the parameter governing the change in viscosity of the colloidal silica was increased by a factor of 30. The infiltration model calibrated with observations from column infiltration experiments provides a simple approach to the design of the secondary containment systems using permeation of colloidal silica. **DOI: [10.1061/(ASCE)EE.1943-7870.0000345](#).** © 2011 American Society of Civil Engineers.

CE Database subject headings: Grouting; Permeability; Infiltration; Containment; Spills; Liquids; Hazardous materials.

Author keywords: Colloidal silica; Grout; Permeation; Infiltration; Secondary containment.

Introduction

Oil and industrial liquids are often stored in aboveground tanks referred to as primary containment systems. The U.S. Environmental Protection Agency (USEPA) estimated that approximately 1.8 million aboveground storage tanks are located in 502,000 onshore facilities within the United States (USEPA 1996). In the event of a failure in the tank or surrounding pipeline network, liquids can be discharged, resulting in a loss of revenue and environmental damage. A secondary containment system, such as the berm shown in Fig. 1, can be constructed around the tank to provide a temporary liquid storage system in the event of an unexpected discharge or catastrophic failure.

Secondary containment has become an important concern in recent years because 84% of the aboveground storage tank facilities do not have low-hydraulic conductivity liners in their secondary containment systems (Hadj-Hamou et al. 2002). In addition, approximately 30% of all leaks that have occurred since 1996 happened at unlined onshore oil facilities or at facilities that did not have a secondary containment system with sufficiently low permeability to contain the spill (USEPA 1996). Secondary containment systems have recently become a mandatory component of hazardous liquid storage facilities to minimize environmental damage resulting from a failure of the primary tank storage system. Specifically, the USEPA issued the *Spill Prevention, Control, and Countermeasure (SPCC) Guidance for Regional Inspectors* (USEPA 2005). This guidance document lists several possible secondary containment systems, which can be used in oil storage facilities to meet the regulations established by CFR 40 Section 112.7(c), but does not provide a prescriptive design. However, the rule indicates that liquid storage facilities should establish a secondary containment system with a liner having a maximum hydraulic conductivity (with the liquid contained as the permeant) ranging from 1×10^{-9} to 1×10^{-7} m/s (or a minimum retention time of 72 h) for the liquids contained. This performance criterion is consistent with American Petroleum Institute (API) standards (USEPA 2005).

An important engineering issue that needs to be addressed is that many aboveground storage tank facilities have extensive pipeline networks surrounding the primary containment facility, preventing earthwork activities or the placement of geosynthetic liners on the ground surface. A solution proposed in this study is the use of permeation grouting to improve the hydraulic properties of the surficial soil layer surrounding the primary containment system. This solution does not require sophisticated equipment and does not interfere with existing pipeline networks. However, it does require the careful consideration of the grout characteristics and infiltration process.

Objectives and Approach

The goal of this study is to develop an infiltration model for predicting the movement of colloidal silica through dry sand, and to

[1]Barry Faculty Fellow and Assistant Professor, Univ. of Colorado at Boulder, Boulder, CO (corresponding author). E-mail: john.mccartney@colorado.edu

[2]Associate Professor, Federal Univ. of Ouro Preto, Minas Gerais, Brazil.

[3]Project Manager, Kleinfelder, Midland, TX.

[4]Fluor Centennial Associate Professor, The Univ. of Texas at Austin, Austin, TX.
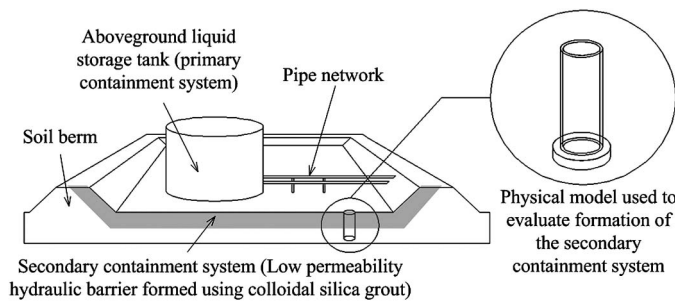
Fig. 1. Secondary containment system and a physical model used to evaluate the process of permeation grouting

develop an experimental infiltration column test that can be used to calibrate the parameters of the infiltration model. The desired outcome from the predictive model is the location of the lower wetting surface and the upper grout surface, which can be used by an engineer to quantify the volume of colloidal silica grout that should be supplied to a soil layer per unit area to create a low permeability hydraulic barrier. The infiltration column tests are needed to account for the uncertainties in the infiltration process that cannot be described by using a simple infiltration model. Specifically, Persoff et al. (1999) and Durmusoglu and Corapcioglu (2000) found that soil-specific interaction is likely to affect the infiltration process of colloidal silica. Furthermore, Karol (2003) observed that permeation grout through dry soils does not occur uniformly but instead by fingering. These two features indicate that a predictive model must be calibrated for a given soil before it can be used to design a secondary containment system.

Background

Mitchell (1981) identified that both cement-based particulate grouts and chemical suspension grouts could be used for permeation applications. Of these, colloidal silica is a chemical suspension grout that has been used in a wide range of soil types to seal leaks in boreholes (Jurinak et al. 1989) and to form hydraulic barriers (Kim and Corapcioglu 2002; Noll et al. 1992, 1993) because of its small particle size, low initial viscosity, controllable and long gel time, nontoxicity, low hydraulic conductivity, relatively low cost, and durability. Colloidal silica is a stable aqueous suspension of colloidal-sized silica particles. The silica particles are produced from saturated solutions of silicic acid and have a diameter ranging from 2 to 100 nm. The colloidal silica suspension will increase in viscosity and eventually form a semisolid gel by increasing the ionic strength of the suspension through the addition of an electrolyte solution or by decreasing the pH. Either action serves to decrease the thickness of the diffuse double layer surrounding the silicate particles, causing interparticle contact bonds to form.

There have been several fundamental studies on the behavior of colloidal silica. Persoff et al. (1999) purposely diluted colloidal silica with distilled water and found that colloidal silica was still able to gel for silica solid concentrations as low as 5%, although the gel time was much longer than for suspensions with higher solid concentrations. Durmusoglu and Corapcioglu (2000) and Persoff et al. (1999) both evaluated the colloidal silica viscosity change as it passed through different soils. Persoff et al. (1999) studied the gel time of colloidal silica in Trevino and Monterey sand #0–30 and found that the colloidal silica in contact with Trevino sand showed a faster gel time. Little effect was observed on the gel time of the colloidal silica when it was placed in contact with Monterey sand #0–30. This was attributed to the high cation exchange capacity of

the Trevino sand particles, the high pH (8.2) of the residual pore fluid in the sand, and the calcium cation content of the soil. Durmusoglu and Corapcioglu (2000) found that the gel time of the colloidal silica when passed through vulcan sand increased by a factor of 3 because of the isomorphic bonding of sodium cations with bivalent calcium ions (thus increasing the ionic strength). Persoff et al. (1999) found that the presence of nonaqueous phase liquids did not influence the gel time, although the presence of aniline led to a faster gel time. Durmusoglu and Corapcioglu (2000) found that colloidal silica in gel form was relatively impermeable to both trichloroethylene and gasoline.

The infiltration process governing the formation of the hydraulic barriers for secondary containment systems by permeation grouting are different from the flow processes described by Gallagher and Koch (2003), Gallagher and Lin (2005), and Lin and Gallagher (2006). The goal of these studies was to characterize colloidal silica in the situation that it is transmitted by groundwater flow to soil layers to reduce their liquefaction potential (Gallagher and Mitchell 2002; Gallagher et al. 2007). In that approach, colloidal silica is diluted to low silica concentrations so that the grout could flow long distances before setting, potentially only forming bonds among soil particle contacts. In contrast, this study focuses on the formation of a near-surface hydraulic barrier with soil pores nearly filled with grout having high silica particle concentrations.

Design of Secondary Containment Systems by Permeation

To meet regulatory requirements, a secondary containment system must meet maximum hydraulic conductivity requirements. For the physical model of the secondary containment system shown in Fig. 2, the addition of colloidal silica grout will create a layer of grouted sand that will have a hydraulic conductivity of less than 10^{-9} m/s (or that the combined grouted and ungrouted portions of the sand layer have an equivalent hydraulic conductivity of less than 10^{-9} m/s). A secondary goal is to ensure that the grout does not gel too early (i.e., before it has passed far enough into the soil profile) or too late (i.e., when it passes too deep into the soil profile or spreads out through diffusion). If the grout gels too early, it will remain on the ground surface and will desiccate. If a finite volume of grout is applied to the ground surface and does not gel quickly enough to set within the soil near the soil surface, the colloidal silica may drain through the soil. The degree of air saturation
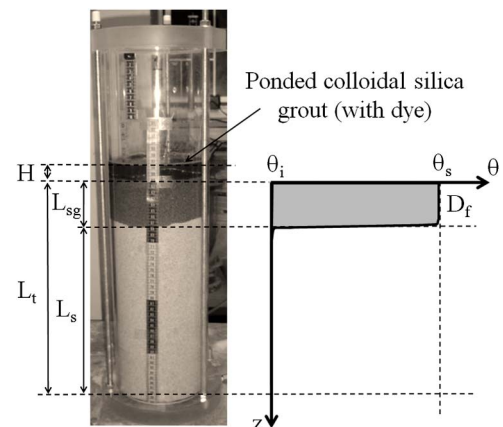
Fig. 2. Geometry variables required for definition of grout volume needed to reach desired system target hydraulic conductivity and for infiltration model (photo courtesy of J. McCartney)

may be relatively high after grouting in this case, implying that grouting would not significantly reduce the hydraulic conductivity of the surface soil. Furthermore, if it does not gel quickly enough, diffusion will lead to the spreading of the grout with depth, preventing the infiltration process of the grout to be modeled by using "plug" flow-type infiltration equations.

Groundwater conditions near a tank will likely vary with time. However, a worst-case scenario for an oil release is an air-dry soil because the oil will not need to surpass the capillary entry pressure for water, which is higher than that for air, to enter the soil. Accordingly, the situation of infiltration into an initially unsaturated soil with a very deep groundwater table (i.e., deep enough that the soil is dry or at residual conditions) will be used as the basis of the model and column tests presented in this paper. The assumption of an initially dry soil profile also simplifies the development of an infiltration model by avoiding the need to consider the effects of grout dilution and pore-water chemistry.

The two parameters that are necessary for the design of secondary containment systems by permeation grouting are the volume of grout to be applied on a unit area of ground surface and the grout dosing ratio (i.e., the ratio of the volume of an accelerator to the total volume of accelerator and colloidal silica). A volume of grout must be selected to (1) ensure the development of a layer of grouted soil thick enough to achieve the required hydraulic conductivity for the system; (2) provide reasonable hydraulic head to push the grout into the unsaturated soil; and (3) ensure that relatively high percentages of grout remain in the soil pores near the surface. The dosing ratio must be carefully selected to provide an optimal gel time that it (1) provides ample time for the mixing and distribution on the surface; (2) permits infiltration to a desired depth; (3) permits gelling before excessive dispersion occurs in the soil profile leading to a heterogeneous soil profile; and (4) prevents excessive grout dilution, which can occur in presence of groundwater. Accordingly, the design requires an approach to estimate the required grout volume that must be supplied to the ground surface and an infiltration model that tracks the movement of grout with different dosing ratios through a soil layer until it gels.

For design purposes, it is useful to assume that the grout is evenly distributed over a sand layer with a length of L_{sg}, as shown in Fig. 2. Equations for the equivalent hydraulic conductivity of a layered soil system, K, can be used to determine the volume of grout needed to form a seepage barrier with thickness L_{sg}, having an acceptable hydraulic conductivity, K_{sg}. The hydraulic conductivity of a layered soil system (Fig. 2) can be obtained by applying a seepage continuity condition as follows:

$$K = \frac{L_t}{\frac{L_s}{K_s} + \frac{L_{sg}}{K_{sg}}} \leq 10^{-9} \text{ m/s} \qquad (1)$$

where K_s = hydraulic conductivity of the initially ungrouted and unsaturated soil; and L_s = difference between the total length of the permeable soil layer, L_t, and the length of grouted soil, L_{sg}. As the total thickness of the permeable soil layer depends on site geometry, Eq. (1) can be arranged to solve for the depth of grouted soil necessary to achieve the required hydraulic conductivity of the system, $K \leq 10^{-9}$ m/s, as follows:

$$L_{sg} = \frac{L_t K_{sg}(K_s - K)}{K(K_s - K_{sg})} \qquad (2)$$

The required volume of grout, V_{grout}, that has to be added to the ground surface can be calculated as follows:

$$V_{\text{grout}} = \theta_{\text{grout}} L_{sg} A \qquad (3)$$

where θ_{grout} = volumetric grout content of the soil after it sets. For simplicity, the model presented in this study assumes that the soil will be fully saturated with grout and so the volumetric grout content equals the porosity of the soil, n. In permeation grouting applications such as the experimental approach conducted as part of this study, this assumption may not necessarily be correct. Specifically, the diffusive spreading of the wetting front during infiltration into an unsaturated soil and two-dimensional infiltration effects (e.g., fingering) may cause a lesser degree of grout saturation.

The volume of grout in Eq. (3) may need to be increased if observations during infiltration indicate that a sufficiently high degree of grout saturation is not obtained. Furthermore, the volume of grout in Eq. (3) may need to be increased to account for the effect of surface drying. In extended dry periods, the surface of the soil will dry, which will lead to a decrease in the hydraulic conductivity of the colloidal silica. The progress of drying fronts through soils grouted with colloidal silica is an issue that has not been investigated in the literature.

Infiltration Model for Permeation of Colloidal Silica

The postgrouting evaluation of the physical models of the secondary containment systems presented in the previous section indicates that the permeation grouting process incorporates several uncertainties. A theoretical model for infiltration is the first step to rationally account for empirical observations. The infiltration Green-Ampt model (Green and Ampt 1911) is simple and commonly used in hydrology to evaluate the infiltration rate and position of the wetting front for different rates of impinging rainfall. One of the major modifications that must be made to the Green-Ampt model is that the hydraulic conductivity of the soil should change with time because of the formation of a gel. Furthermore, the Green-Ampt model should be modified to account for the infiltration of a discrete volume of grout applied to the ground surface (i.e., a falling-head boundary condition), which is not a common analysis in hydrology.

It is assumed that the infiltration of colloidal silica obeys Darcy's law as follows:

$$f = -K_{sg}(t)\frac{dh}{dz} \qquad (4)$$

where f = infiltration rate; dh/dz = gradient in hydraulic total head; and $K_{sg}(t)$ = hydraulic conductivity of the soil layer to the grout. The value of $K_{sg}(t)$ is a function of time because the colloidal silica experiences an increase in dynamic viscosity during gelation. The change in the hydraulic conductivity of the soil to grout can be modeled by using a form of the Kozeny-Carman equation (Mitchell and Soga 2005), which incorporates an exponential growth in dynamic viscosity as follows:

$$K_{sg}(t) = \frac{\kappa\gamma_{cs}}{\mu(t)} = \frac{\kappa\gamma_{cs}}{\mu_0 e^{\beta t}} = \frac{\kappa\gamma_{cs}}{\mu_0}e^{-\beta t} \qquad (5)$$

where μ_0 = initial dynamic viscosity; β = exponential growth coefficient; κ = intrinsic permeability of the soil; and γ_{cs} = unit weight of the colloidal silica grout. In this model, it is assumed that the intrinsic permeability of the soil and the unit weight of the colloidal silica are constant with time during the gelation of the colloidal silica.

The key assumption of the Green-Ampt model is that colloidal silica flows through the soil as a plug with a sharply defined wetting front, as shown in Fig. 2. The hydraulic gradient is determined by using the total head values at the ground surface (i.e., the point of infiltration) and at the wetting front. Assuming the vertical spatial

coordinate, z, as positive in the downward direction from the surface and a negative pressure head at the wetting front equal to $h_p = u_w/\gamma_w = -\psi_f/\gamma_w = -\Psi_f$, the hydraulic gradient can be written as

$$\frac{dh}{dz} = \frac{h_{\text{wettingfront}} - h_{\text{surface}}}{z_{\text{wettingfront}} - z_{\text{surface}}} = \frac{(D_f - \Psi_f) - (H - 0)}{D_f} = 1 - \frac{H + \Psi_f}{D_f}$$
(6)

where H = height of the upper surface from the ground surface; D_f = depth of the wetting front; and Ψ_f = suction head at the wetting front. The value of H may be positive or negative depending on whether the upper surface of the grout is above the ground surface (ponding) or beneath the ground surface.

In conventional applications of the Green-Ampt model, the position of the wetting front is calculated first by setting the impinging rainfall rate equal to the infiltration rate in the case that surface ponding has not occurred ($H = 0$). A similar approach can be used for the infiltration of colloidal silica, although the primary difference is that ponding is started immediately. Accordingly, the cumulative volume of grout per unit area, F, that has infiltrated into the ground (Fig. 2) is related to the depth of the wetting front and the difference in water content, $\Delta\theta$, as follows:

$$F = (n - \theta_i)D_f = \Delta\theta D_f$$
(7)

As mentioned in the previous section, the volume of colloidal silica needed to create a layered system with an equivalent hydraulic conductivity less than 10^{-9} m/s can be referred to as the maximum cumulative infiltration volume per unit area, F_{max}, of the secondary containment system. In other words, all the colloidal silica grout applied to the surface should enter the ground. The value of F_{max} is closely related to the height of ponding. Initially, water will pond on the ground surface, theoretically to a height $H = F_{\text{max}}$. After this, the height of ponding, H, is equal to

$$H = F_{\text{max}} - F$$
(8)

where F = portion of the total volume per unit of area, F_{max}, that has entered the soil. Mein and Larson (1973) were the first to incorporate a time-dependent decrease in ponding height atop the soil layer. It is possible for the height of ponding on the grout surface to pass into the soil because the Green-Ampt model treats infiltration as plug flow. The position of the upper grout surface can be inferred from H, although the grout surface passes below the soil surface, it must be multiplied by the porosity of the soil to account for the balance of mass.

Expressing the hydraulic gradient [Eq. (6)] as the cumulative volume of infiltrated grout per unit area, F, by using the Eqs. (7) and (8) and by using the time-dependent relation for the hydraulic conductivity of the soil to grout [Eq. (5)], the infiltration rate of colloidal silica in Eq. (4) can be rewritten as follows:

$$f = -\frac{\kappa\gamma_{cs}}{\mu_0}e^{-\beta t}\left[1 - \frac{\Delta\theta(F_{\text{max}} - F + \Psi_f)}{F}\right]$$
(9)

Now considering that the infiltration rate [Eq. (9)] is also equal to the volume of grout infiltrated across the upper surface of the soil per unit area per unit of time (i.e., dF/dt), the following differential form of the Green-Ampt equation for the infiltration of a discrete volume of colloidal silica into a soil layer can be obtained:

$$\frac{dF}{dt} = -\frac{\kappa\gamma_{cs}}{\mu_0}e^{-\beta t}\left[\frac{F(1 + \Delta\theta) - \Delta\theta(F_{\text{max}} + \Psi_f)}{F}\right]$$
(10)

By using the separation of variables technique, the differential Eq. (10) can be solved by

$$F_{i+1} = F_i + (1 + \Delta\theta)\left[\frac{\kappa\gamma_{cs}}{\beta\mu_0}\left(e^{-\beta t_{i+1}} - e^{-\beta t_i}\right)\right]$$
$$+ \frac{\Delta\theta(F_{\text{max}} + \Psi_f)}{(1 + \Delta\theta)}$$
$$\times \left\{\ln\left[\frac{\Delta\theta(F_{\text{max}} + \Psi_f) - (1 + \Delta\theta)F_i}{\Delta\theta(F_{\text{max}} + \Psi_f) - (1 + \Delta\theta)F_{i+1}}\right]\right\} +$$
(11)

where F_{i+1} and F_i = values of F at times i and $i + 1$. Eq. (11) is referred to as the implicit form of the Green-Ampt equation. An implicit solver can be used to iteratively determine F with successive time steps. The depth of the wetting front, D_f, can be calculated by using Eq. (7), and the position of the upper surface of grout, H, can be calculated by using Eq. (8).

Materials and Methods

Sand

Lapis-lustre Monterey sand #0–30 was used in the column study to evaluate the permeation of colloidal silica. This soil, classified as SP in the Unified Soil Classification system, was selected as it is clean, uniformly graded, and predominantly consisting of quartz with a smaller amount of feldspars and other minerals, making it relatively inert. A mechanical sieve analysis following ASTM D422 (ASTM 2007b) was conducted on the Monterey #0–30 sand to determine the particle size distribution, the results of which are shown in Fig. 3(a). The particle size distribution indicates that 99.9% of the Monterey #0–30 is composed of sand-size particles (i.e., ranging from 0.075 to 5 mm). The coefficient of curvature, C_c, is 0.95, and the coefficient of uniformity, C_u, is 1.76. A target relative density of 50% was used in this study for all infiltration
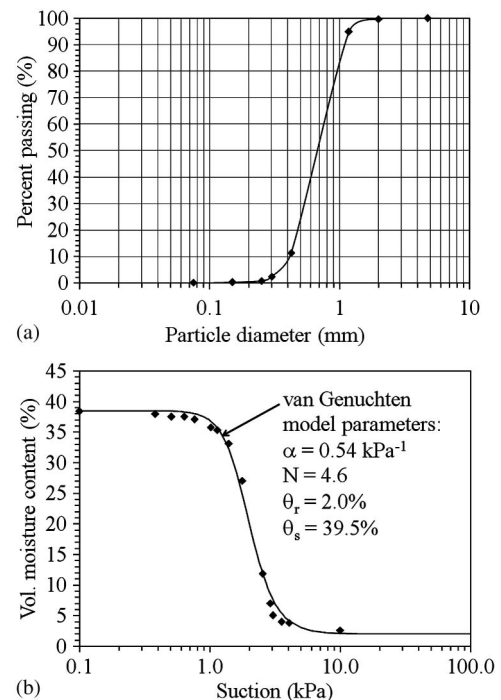
Fig. 3. Monterey sand #0–30 characteristics: (a) gradation curve; (b) soil-water retention curve

and hydraulic characterization tests. This corresponds to a porosity of 0.395 and a void ratio of 0.67. The maximum and minimum void ratios for the sand are 0.78 and 0.56, respectively (Li 2005). The specific gravity of this sand was found to be 2.65. Although a relative density of 50% is relatively loose, it replicates a worst-case situation from the perspective of permeability for the surficial soil in the secondary containment system.

The hydraulic conductivity of the water-saturated sand was determined by using a constant head permeameter test (ASTM 2007a). Dry sand was placed to a relative density of 50% by vibrating four 3.2 cm lifts in a rigid-wall permeameter, and flow was applied under gradients ranging from 1 to 7. The hydraulic conductivity of the saturated sand was found to be 5.29×10^{-4} m/s. The soil-water retention curve (SWRC) of the sand was determined by using the hanging column test (ASTM 2008, "Approach A"). The SWRC data, along with a best-fit curve from the van Genuchten model (1980), are shown in Fig. 3(b). The SWRC shows that the soil has a steep decrease in water content from saturated to dry conditions at the air-entry suction of 1.6 kPa. The infiltration tests performed in this study were conducted in sand that was initially under air-dry conditions with a hygroscopic volumetric water content of 2.0%. The initial suction in the sand was not measured, but it is likely that the suction at the wetting front during infiltration is greater than the suction corresponding to residual saturations (10 kPa, corresponding to a suction head of $\Psi_f = 1$ m).

Colloidal Silica

The colloidal silica grout used in this research is commercially known as MEYCO MP320T (Eka Chemicals 2006). This colloidal silica is a "one component" grout, indicates that the colloidal silica grout is mixed with an accelerator at a selected dosing ratio before injection. The accelerator used in this study was prepared by

mixing 1 kg of table salt with 9 kg of distilled water. Table salt contains several minerals, so its performance as an accelerator will likely be different from the pure NaCl accelerators used in other studies (Persoff et al. 1999) and in engineering practice. Nonetheless, it was still found to function well as an accelerator. The gel time of the colloidal silica was be controlled by varying the amount of accelerator added to the colloidal silica suspension. The dosing ratio, R_d, was defined in this study as the volume of accelerator (i.e., saltwater mixture) divided by the total volume of the mixture (i.e., accelerator and suspension) and is expressed as a percentage. In this study, a mixture with 13% accelerator is referred to as "colloidal silica with $R_d = 13\%$." Although the actual variable that controls the gel time is the concentration of sodium in the mixture, the dosing ratio was used because of its relative simplicity.

The colloidal silica contains approximately 30% silica solids by weight. A Brookfield Thermoset viscometer was used to measure the dynamic viscosity of colloidal silica solutions under room temperature conditions. The colloidal silica suspension before addition of the accelerator had a pH of 9.5, a density of 1,200 kg/m^3, and a dynamic viscosity of 0.01 kg/ms. The accelerator, which had a density of 1,200 kg/m^3 and a neutral pH of 7, was found to have a dynamic viscosity of 0.001 kg/ms. The resulting mixture proved to have an initial dynamic viscosity ranging from 0.03 to 0.06 kg/ms, a pH of 8, and a density of 1,150 kg/m^3 (Eka Chemicals 2006). The initial properties of the colloidal silica before gelling are only an order of magnitude greater than those of water (i.e., a dynamic viscosity of 0.001 kg/ms). The changes in dynamic viscosity with time for colloidal silica mixtures with dosing ratios ranging from 5 to 17% are shown in Fig. 4(a). The gel time was defined in this study as the time required to reach a dynamic viscosity of 9 kg/ms, which is considered the boundary between liquid and gel stages (Karol 2003). The gel time for the colloidal silica having different dosing ratios of the table salt accelerator is
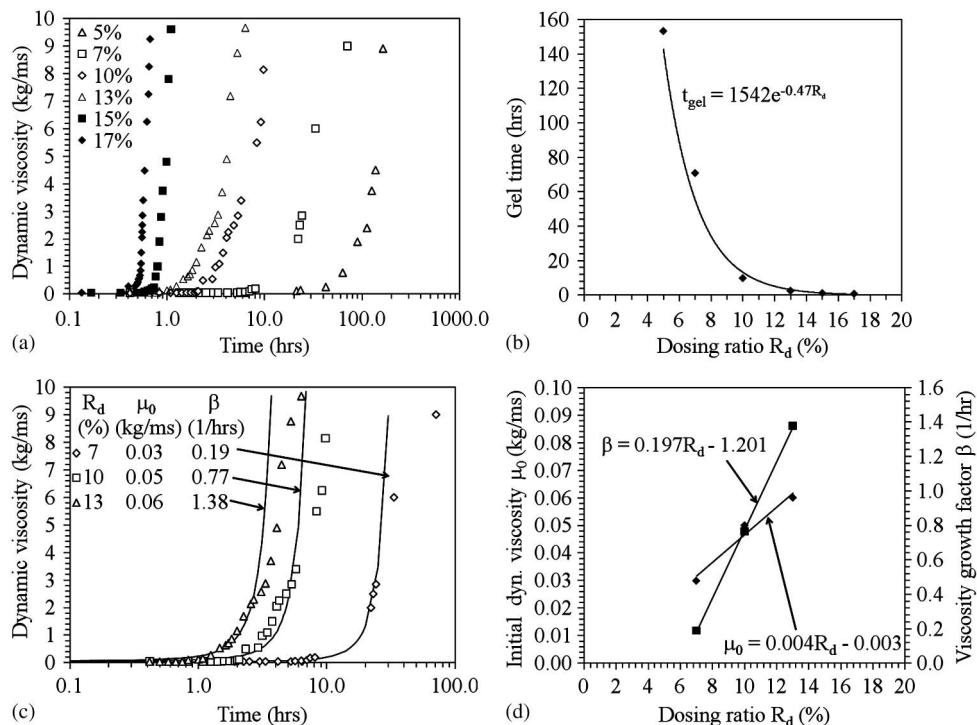
Fig. 4. Dosing ratio influence on colloidal silica properties: (a) grout viscosity with time after addition of accelerator; (b) variation in gel time with accelerator dosing ratio; (c) viscosity-time model fitted to the experimental viscosity data; (d) variation in viscosity-time model parameters with dosing ratio

shown in Fig. 4(b). It ranged from approximately 40 min for $R_d = 17\%$ to 153 h for $R_d = 5\%$.

It was not possible to use the viscometer to assess the increase in dynamic viscosity with time after the infiltration of the colloidal silica into the Monterey sand. Instead, specimens of sand mixed uniformly with colloidal silica having $R_d = 13\%$ were prepared in a split mold system. A pocket penetrometer was used to infer the change in stiffness of the sand-colloidal silica as a function of time, which was assumed to be associated with the in-soil gel time of the colloidal silica. The approximate gel time was found to be 35% shorter than that reported in Fig. 4(b). This finding contradicts the gel times reported by Persoff et al. (1999) for colloidal silica in Monterey sand #0–30, likely because of the difference in accelerator. Persoff et al. (1999) used NaCl whereas table salt was used in this study. The change in the gel time of the colloidal silica in the presence of soil could also be attributable to the surface effects encountered during the wetting of the initially dry sand particles.

The dynamic viscosity increase curves in Fig. 4(a) were fitted with the exponential growth model incorporated into the definition of the hydraulic conductivity of soil to colloidal silica, given by

$$\mu = \mu_0 e^{\beta t} \tag{12}$$

where μ_0 = initial dynamic viscosity value for small times; and β = exponential growth term. The fitted trends and parameters are shown in Fig. 4(c) for colloidal silica having $R_d = 7$, 10, and 13%. The other colloidal silica specimens with different dosing ratios were removed from this analysis because their set times were either too fast (i.e., less than 1 hour for colloidal silica having $R_d = 15$ and 17%) or too slow (i.e., more than 100 h for colloidal silica having $R_d = 5\%$). A least-squares regression was used to fit the curves to the experimental data in Fig. 4(c) for values of time near the beginning of the increase in viscosity. The best-fit parameters for colloidal silica having $R_d = 7$, 10, and 13% are shown in Fig. 4(d). A linear trend is observed between the dosing ratio, R_d, and the parameters μ_0 and β.

The hydraulic conductivity values for monolithic specimens of gelled colloidal silica having different dosing ratios were determined in flexible wall permeameter tests. An effective stress of 20.7 kPa was placed on the specimens of colloidal silica, which resulted in a volumetric strain of approximately 20%. Persoff et al. (1999) found that colloidal silica was prevented from consolidating under a change in effective stress when in sand, so it is likely that the value of hydraulic conductivity of the monolithic colloidal silica is less than that in grouted sand. Nonetheless, the hydraulic conductivity of the monolithic colloidal silica to water was found to be 5.6×10^{-12} m/s and was not sensitive to the dosing ratio. Although the hydraulic conductivity of monolithic colloidal silica to water is low when submerged, it was found to be prone to significant desiccation upon drying. This indicates that a hydraulic barrier created by using the infiltration of colloidal silica into a soil layer should not result in monolithic colloidal silica too close to the soil surface.

The hydraulic conductivity values of specimens of sand mixed with colloidal silica grout having different dosing ratios were also assessed. Dry sand was mixed with a volume of colloidal silica grout estimated to completely fill the void space. Wet tamping was then used to reach the target relative density of 50% in a split-shell compaction mold, after which the grout was permitted to gel for 1 week in a humidity controlled chamber. The hydraulic conductivity of the grouted sand was found to be comparatively insensitive to the dosing ratio under an effective stress of 20.7 kPa with a magnitude of approximately 3×10^{10} m/s. The hydraulic

conductivity of the grouted sand is less than the performance criterion (i.e., 10^{-9} m/s) for secondary containment systems, but is greater than that of the monolithic colloidal silica because the structure of the sand prevents the consolidation of colloidal silica under the applied effective stress (Persoff et al. 1999). Although water was used as the permeant to check the hydraulic conductivity of the grouted sand, other studies indicate that colloidal silica is compatible with nonaqueous phase liquids (NAPLs) (Durmusoglu and Corapcioglu 2000).

The uniformly mixed specimens of grouted sand may not represent the sand grouted in an infiltration test in the laboratory or field. In the field, greater amounts of air and higher hydraulic conductivity values, on average, exist. Nonetheless, it provides a baseline to evaluate the effect of the dosing ratio on sand specimens that have a degree of grout saturation of 100%. The desiccation behavior noted for monolithic colloidal silica specimens when left exposed was not noted for the grouted sand specimens, although the hydraulic conductivity of the dried colloidal silica within the soil pores certainly increased.

The time-dependent increase in viscosity of the colloidal silica will lead to a decrease in the hydraulic conductivity of the sand to the grout with time. This effect can be highlighted by applying the Eq. (5), considering the unit weight of the colloidal silica, γ_{cs}, equals approximately 11.5 kN/m^3; and the linear functions for the μ_0 and β parameters [Fig. 4(d)] and the intrinsic permeability of soil, κ, are 5.39×10^{-11} m^2. It is important to mention that the intrinsic permeability of the soil, κ, which does not depend on the liquid properties, was obtained by applying Eq. (5), adopting a unit weight of water of 9.81 kN/m^3, a dynamic viscosity of water of 0.001 kg/ms, and a saturated hydraulic conductivity of 5.29×10^{-4} m/s for Monterey sand ($D_r = 50\%$).

The hydraulic conductivity of Monterey sand #0–30 to colloidal silica having $R_d = 7$, 10, and 13% as a function of time, predicted by using Eq. (5) are shown in Fig. 5. The hydraulic conductivity of the sand to the grout is initially relatively constant, but then decreases exponentially as the grout begins to gel. This analysis is valid for soil that is fully saturated with colloidal silica.

Infiltration Column Testing for Permeation Grouting

The container used to form the physical model of a secondary containment system was a 150 mm diameter rigid-wall acrylic permeameter having a height of 600 mm, as shown in Fig. 6. The height of the permeameter was selected on the basis of the column infiltration testing experience of McCartney et al. (2005) to ensure that the soil layer within the permeameter has sufficient thickness to minimize the influence of the bottom boundary on the grout infiltration process. The diameter was selected so that the grouted soil could be
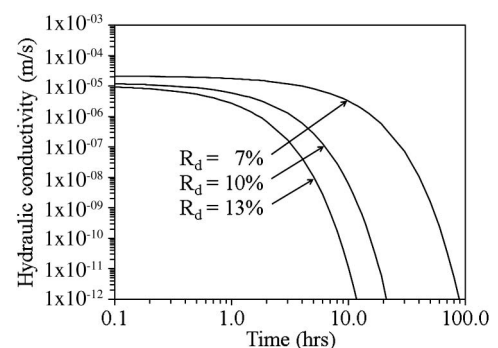
Fig. 5. Prediction of time-dependent change in hydraulic conductivity of sand during grout gelation
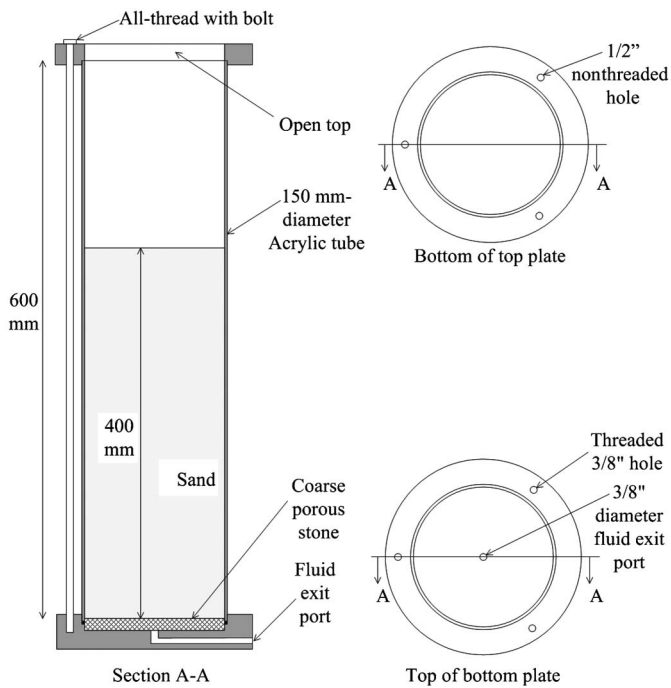
Fig. 6. Permeameter used for infiltration testing

Fig. 7. Average depth of colloidal silica infiltration measured by using visual observations with time for different dosing ratios

easily exhumed after infiltration. The top of the permeameter was open, which permitted the placement of the sand layer, permeation of the grout through the sand surface, and the postgrouting evaluation of the hydraulic conductivity of the sand-grout system. The base of the permeameter consisted of a metal screen underlain by a fluid exit port. As this study focuses on the improvement of surface soils, the permeameter did not incorporate an overburden pressure.

Three physical models of secondary containment systems were constructed in the column permeameter, as shown in Fig. 6, each evaluated by using the same volume of colloidal silica, but having different dosing ratios of 7, 10, and 13%. The column was assembled, placed atop a vibratory shaking table, filled with dry-sand layers of 50 mm, and vibrated to reach the relative density of 50%. The total soil layer thickness of each of the columns was equal to 400 mm. The bottom exit port was opened to permit the free outflow of air during infiltration. Approximately 900 ml of grout was then added to the surface of the sand layer, which based on the analysis in the previous section, should be sufficient to lead to a layer with a thickness L_{sg} of 127 mm, considering the soil fully filled by grout). A slotted plastic screen was placed above the sand surface to help dissipate the energy of pouring the grout onto the sand surface. A red tracer with low diffusivity (i.e., Rhodamine WT) was added to the grout to help track its movement through the soil profile. The downward progress of the grout was tracked visually on the sides of the permeameter by using four tape measures.

Experimental Results

The average depth of the wetting front in each column was measured by using visual observations of the dyed grout through the acrylic wall of the permeameter, as shown in Fig. 7. For colloidal silica having $R_d = 7\%$, the wetting front reached the base of the profile (i.e., 400 mm), and a negligible volume of grout was observed to leak from the outflow port (i.e., about 1% of the infiltrated volume of grout). However, for colloidal silica having $R_d = 10$ and
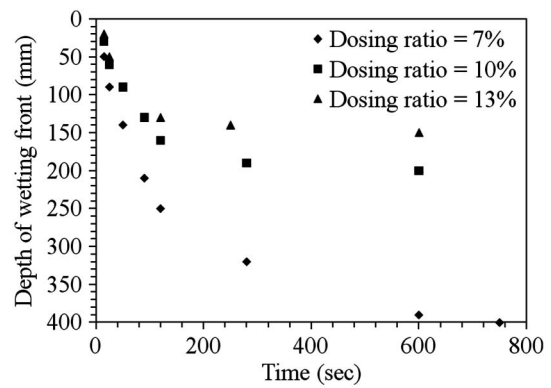
13%, the wetting front was observed to stop at depths of 200 and 150 mm, respectively. These results are in accordance with the observed gel time and hydraulic conductivity in Figs. 4(b) and 5, respectively. The colloidal silica having $R_d = 7\%$ had the longest gel time, so it was able to travel the furthest from the soil surface before gelling.

After permitting the grout to set within the columns, 100 cm of water was added to the top of the soil profiles to evaluate the integrity of the hydraulic barriers formed in the soil layers. All three hydraulic barriers were found to retain water for a period of 72 h, and the measurable outflow of water was noted only in the case of the column grouted with colloidal silica having $R_d = 13\%$. Although the fluids that a secondary containment system would encounter will certainly be different than water, water is still useful to evaluate the hydraulic integrity of the barrier. If the barrier has integrity, and the permeant is compatible with the colloidal silica, the barrier should serve its purpose. Durmusoglu and Corapcioglu (2000) found that the hydraulic barriers formed with colloidal silica are chemically compatible with NAPLs such as gasoline and TCE.

To evaluate the actual distribution in colloidal silica with depth, the grouted profiles were slowly extruded from the base of the profile, as shown in Fig. 8(a). The grouted soil was pushed from the column in 50 mm segments, as shown in Fig. 8(b), and the percentage of grouted sand by dry mass was measured. In the case that the sand throughout the profile contained enough grout to remain intact (i.e., for $R_d = 7\%$), each 50 mm segment was weighed to calculate the density. The measured density can be compared to the expected density of a segment fully saturated with grout to estimate the degree of grout saturation. In the case that a more distinct contrast was observed between grouted and loose sand (i.e., for $R_d = 10$ and 13%), the loose, dry sand was removed and weighed. This left the intact grouted sand mass shown in Fig. 8(c). In the case of the profiles grouted with colloidal silica having $R_d = 10$ and 13%, the entire grouted masses were removed from the column, as shown in Fig. 8(d). After taking photographs, the mass density of the uniformly grouted layers of soil near the surface of the profiles were measured and compared with the values that would have been obtained for a 100% degree of grout saturation. The grouted "fingers" observed in Fig. 8(d) were only encountered for the colloidal silica having $R_d = 10$ and 13%; most of the grout for the colloidal silica having $R_d = 7\%$ was found to have infiltrated to the bottom of the profile. In all three columns, no indication of preferential seepage along the column walls was noted during the exhumation process.

The variation of the degree of grout saturation with depth is shown in Fig. 8(e). The circle in Fig. 8(e) shows the maximum depth of the wetting front observed in Fig. 7. The sand layer

(a)　　　　　(b)

(c)　　　　　(d)

(e)
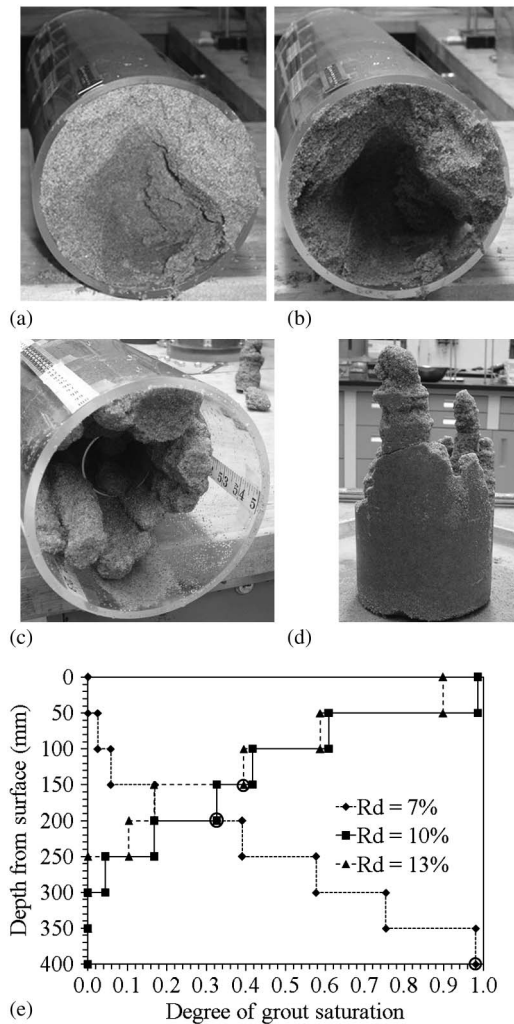
Fig. 8. Postinfiltration evaluation results: (a) extrusion of sand column until grouted soil appears; (b) excavation of loose sand from around grout fingers; (c) exposure of grout fingers and embedded metal rings; (d) removal of grouted sand from column; (e) degree of grout saturation in the sand column; circles denote the depth of the wetting front (photos courtesy of J. McCartney)

grouted by using colloidal silica having $R_d = 7\%$ showed the widest distribution of grout throughout the soil profile, with the greatest volume of grout near the outflow face of the column. The sand columns grouted with colloidal silica having $R_d = 7$ and 10% were found to function satisfactorily as a secondary containment layer, likely because both of these columns had zones with degrees of grout saturation on the order of 98%, albeit on opposite ends of their respective columns. On the other hand, the column grouted by using colloidal silica having $R_d = 13\%$ experienced some leakage of water, likely because the degree of grout saturation was only 89% near the surface of the soil.

The profiles grouted by using colloidal silica having $R_d = 10$ and 13% showed uniform layers of grouted sand, up to the depths of the wetting fronts measured by using visual observation. However, fingers were observed to extend to a depth of 300 mm for colloidal silica having $R_d = 10\%$ and to a depth of 250 mm for colloidal silica having $R_d = 13\%$. It is possible that the fingering contributed to the lesser degree of grout saturation in the profiles grouted by using colloidal silica having $R_d = 13\%$. Nevertheless, despite the issues with fingering and lesser degree of grout

saturation, the sand profiles grouted by using colloidal silica having $R_d = 13\%$ showed the desired behavior expected in the hypothetical design scenario for secondary containment systems described previously. An increased volume of colloidal silica applied during the permeation process would have led to a uniform surface hydraulic barrier having a higher degree of grout saturation.

Analysis

The first objective of the infiltration model was to quantify the location of the wetting front. To do so, most of the parameters in Eq. (11) can be defined in a straightforward manner. The hydraulic conductivity parameters in Eq. (11) were defined from the experimental results shown in Fig. 4(d), whereas the initial volumetric water content was set to the hygroscopic volumetric water content of approximately 2%, so $\Delta\theta$ was equal to 0.39. The only parameter that is difficult to determine is the suction head at the wetting front. Comparisons of rigorous infiltration models and the Green-Ampt model indicate that the wetting front typically does not follow a sharp contrast in the volumetric water content, as shown in Fig. 2. Accordingly, even if the suction at the wetting front were to be measured, its use in the Green-Ampt model may not lead to an appropriate quantification of the infiltration process. As it was not possible to estimate an appropriate value of Ψ_f for the modified Green-Ampt model, a criterion was set that the value of Ψ_f should be greater than 1 m. Suction heads greater than this value represent residual saturation conditions of the dry sand on the basis of the SWRC in Fig. 3(b). It was not possible to use regression to define the value of Ψ_f to best represent the depth of the wetting front because the measured depth of the wetting front showed a slight delay after pouring the grout onto the sand surface. Nonetheless, a value of Ψ_f of 4 m, corresponding to a suction of 40 kPa, was found to provide a good estimate of the slopes of the wetting front depth curves with time, as shown in Fig. 9(a).

Although the model results show a slight decrease in the rate of the wetting front with time consistent with the increase in viscosity of the grout, it does not provide a good fit to the data for time values greater than 150 s. Specifically, the model tends to overpredict the depth of the wetting front, likely because the colloidal silica gelled in the soil faster than observed in the viscosity measurements made in Fig. 4(a). Furthermore, the model did not predict an asymptotic trend in the depth of the wetting front, indicating the formation of a uniform layer of grouted sand. The position of the upper surface of the grout, H, calculated by using Eq. (8), is shown in Fig. 9(b). The trend in H with time indicates that the grout "plugs" are continuing to pass through the soil layer after 800 s, and that the soil grouted by using colloidal silica having $R_d = 7\%$ has completely passed through the soil layer after approximately 580 s. In this case, the model neglects the diffusive spreading of the wetting front and the upper surface of the grout that was observed in the spatial distribution of colloidal silica having $R_d = 7\%$, as shown in Fig. 8(e).

The differences in the wetting front location predicted by the model and observed in the infiltration column test are attributable to the soil-specific interaction with the colloidal silica, leading to an increase in the rate of exponential growth in its viscosity, and attributable to the infiltration of the grout by fingering. When the values of β for the three dosing ratios (i.e., $R_d = 7$, 10, and 13%) were increased by a factor of 30, a good fit was obtained to the wetting front measurements, as shown in Fig. 10(a). This larger value of β corresponds a decrease in the gel time of approximately 33%, which is very close to the shorter time required for the gelling of the colloidal silica specimens mixed with sand. Furthermore,
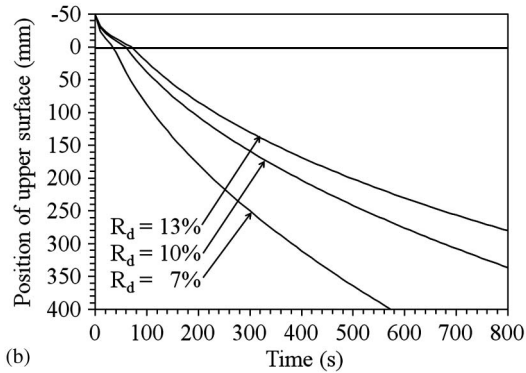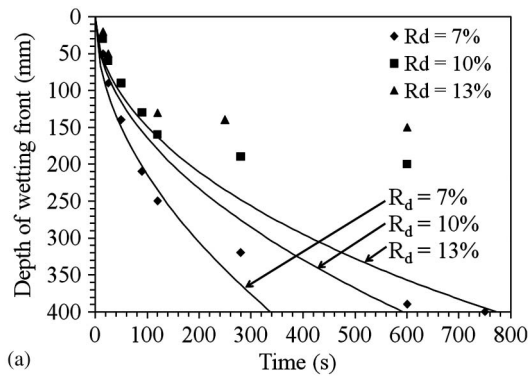
Fig. 9. Comparison of results from infiltration experiment with those from model with measured parameters: (a) depth of wetting (lower) surface of grout "plug" during infiltration; (b) depth of upper surface of grout "plug" during infiltration
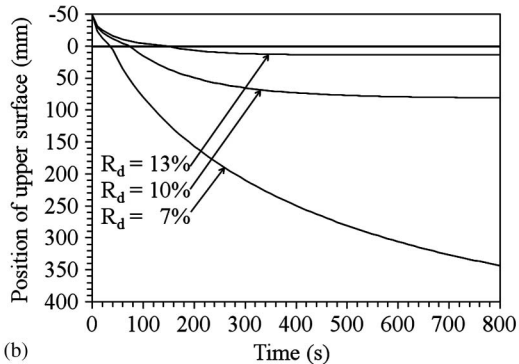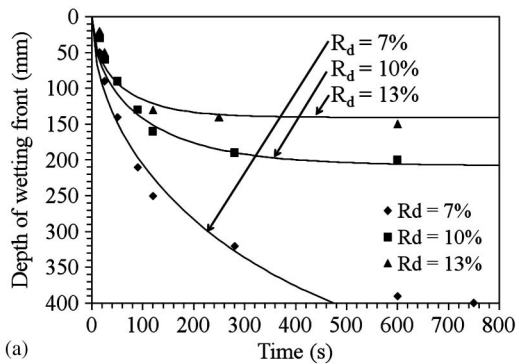
Fig. 10. Calibration of model against results from infiltration experiment by incorporating greater rate of increase in viscosity: (a) depth of wetting (lower) surface of grout "plug" during infiltration; (b) depth of upper surface of grout "plug" during infiltration

the position of the upper surface of the grout for the adjusted rate of increase in viscosity, shown in Fig. 10(b), is also more consistent with the distributions in colloidal silica having different dosing ratios, as shown in Fig. 8(e). In this manner, the infiltration column test can be used on a project to calibrate the model parameters for the infiltration model. The calibrated infiltration model can then be used to design the hydraulic barrier.

Although the adjusted model is capable of fitting the observed wetting front trends, it does not ensure that adequate hydraulic improvement will be obtained. The wetting fronts for the colloidal silica having different dosing ratios reached the target depth, but the degree of grout saturation in this zone was not equal to 1.0. A simplistic approach to solve this problem would be to add a volume of grout equal to the difference between the porosity and the volumetric grout content to the total volume of infiltration predicted by using Eq. (3), or approximately 10% more. This approach may be improved in the future by (1) quantifying the hydraulic conductivity of soil having different degrees of grout saturation; and (2) improving the sophistication of the infiltration model to better consider the degree of grout saturation with depth (i.e., a diffuse wetting front).

Conclusions

Colloidal silica grout can be used to improve soils around aboveground tanks to form a secondary containment system through surface permeation because of its low initial viscosity and controllable gel time. An infiltration model for colloidal silica was presented in this study that considered the effects of the change in grout viscosity with time for different dosing ratios of accelerator (i.e., a saltwater solution). The infiltration of colloidal silica having different dosing ratios into a 400 mm long sand column was found to lead to a wetting front that decreased in velocity with time because of the time-dependent increase in viscosity of the colloidal silica. Colloidal silica having a dosing ratio of 7% was observed to solidify near the bottom of the soil profile, leaving behind a trail of colloidal silica having a relatively low degree of grout saturation. Colloidal silica having dosing ratios of 10 and 13% were observed to form a uniformly grouted sand layer near the surface with a high degree of grout saturation, with infiltration extending deeper into the soil profile by fingers. Although the soil profiles grouted with colloidal silica having dosing ratios of 7 and 10% were found to retain water for 24 h after gelling, the column grouted with colloidal silica having a dosing ratio of 13% experienced some leakage of water. This was attributed to the lesser degree of grout saturation near the soil surface for this column. The results of the physical modeling tests involving the infiltration of colloidal silica into sand layers indicate that soil-specific issues lead to differences between the predicted and measured depths of grout infiltration with time. This observation emphasizes that the predictive model should be used along with soil-specific infiltration tests to calibrate model parameters.

Acknowledgments

References

ASTM. (2007a) "Standard test method for measurement of hydraulic conductivity of porous material using a rigid-wall, compaction-mold permeameter." *D5856*, West Conshohocken, PA.

ASTM. (2007b). "Standard test method for particle-size analysis of soils." *D422*, West Conshohocken, PA.

ASTM. (2008). "Standard test methods for determination of the soil water characteristic curve for desorption using a hanging column, pressure extractor, chilled mirror hygrometer, and/or centrifuge." *D6836*, West Conshohocken, PA.

Durmusoglu, E., and Corapcioglu, M. Y. (2000). "Experimental study of horizontal barrier formation by colloidal silica." *J. Environ. Eng.*, 126(9), 833–841.

Gallagher, P. M., Conlee, C. T., and Rollins, K. M. (2007). "Full-scale field testing of colloidal silica grouting for mitigation of liquefaction risk." *J. Geotech. Geoenviron. Eng.*, 133(2), 186–196.

Gallagher, P. M., and Koch, A. J. (2003). "Model testing of passive site stabilization: A new grouting technique." *Grouting and Ground Treatment: Proc., 3rd Int. Conf.*, ASCE, Reston, VA, 1478–1489.

Gallagher, P. M., and Lin, Y. (2005). "Column testing to determine colloidal silica transport mechanisms." *Proc., GSP 136: Innovations in Grouting and Soil Improvement, Geo-Frontiers 2005 Congress*, ASCE, Reston, VA, 15–26.

Gallagher, P. M., and Mitchell, J. K. (2002). "Influence of colloidal silica grout on liquefaction potential and cyclic undrained behavior of loose sand." *Soil Dyn. Earthquake Eng.*, 22(9–12), 1017–1026.

Green, W. H., and Ampt, G. A. (1911). "Studies on soil physics: 1. Flow of air and water through soils." *J. Agric. Sci.*, 4(1), 1–24.

Hadj-Hamou, T., Myers, P., and Sanglerat, T. (2002). "Alternatives to secondary containment lining." *Proc., Freshwater Spills Symp.*, U.S. Environmental Protection Agency (USEPA), Washington, DC.

Jurinak, J. J., Summers, L. E., and Bennett, K. E. (1989). "Oilfield applications of colloidal silica gel." *Proc., Int. Symp. on Oil Field Chemistry*, Society of Petroleum Engineers, Richardson, TX.

Karol, R. (2003). *Chemical grouting and soil stabilization*, 3rd Ed., Marcel Dekker, Basel, Switzerland.

Kim, M., and Corapcioglu, M. Y. (2002). "Modeling of gel barrier formation by using horizontal wells." *J. Environ. Eng.*, 128(10), 929–941.

Li, C. (2005). "Mechanical response of fiber reinforcement soil." Ph.D. dissertation, The Univ. of Texas at Austin, Austin, TX.

Lin, Y., and Gallagher, P. M. (2006). "Three-meter column testing of colloidal silica transport through porous media." *Proc., GSP 152: Ground Modification and Seismic Mitigation*, ASCE, Reston, VA, 417–424.

McCartney, J. S., Kuhn, J. A., and Zornberg, J. G. (2005). "Geosynthetic drainage layers in contact with unsaturated soils." *Proc., 16th ISSMGE Conf.: Geotechnical Engineering in Harmony with the Global Environment*, International Society for Soil Mechanics and Geotechnical Engineering, London.

Mein, R. G., and Larson, C. L. (1973). "Modeling infiltration during a steady rain." *Water Resour. Res.*, 9(2), 384–394.

MEYCO Global Underground Construction. (2009). "MEYCO MP 320 T: Solvent-free, low viscosity, hydrophilic grout for rock injection and consolidation of sand and silt strata." BASF Construction Chemicals Europe, Zurich, Switzerland.

Mitchell, J. K. (1981). "Soil improvement: State-of-the-art report." *Proc., 10th Int. Conf. on Soil Mechanics and Foundation Engineering*, Taylor and Francis, London, 509–565.

Mitchell, J. K., and Soga, K. (2005). *Fundamentals of soil behavior*, 3rd Ed., Wiley, Hoboken, NJ.

Noll, M. R., Bartlett, C., and Dochat, T. M. (1992). "In situ permeability reduction and chemical fixation using colloidal silica." *Proc., Sixth National Outdoor Action Conf.*, National Groundwater Association, Westerville, OH, 443–457.

Noll, M. R., Epps, D. E., Bartlett, C. L., and Chen, P. J. (1993). "Pilot field application of a colloidal silica gel technology for in situ hot spot stabilization and horizontal grouting." *Proc., Seventh National Outdoor Action Conf.*, National Groundwater Association, Westerville, OH, 207–219.

Persoff, P., Apps, J., Moridis, G., and Whang, J. M. (1999). "Effect of dilution and contaminants on sand grouted with colloidal silica." *J. Geotech. Geoenviron. Eng.*, 125(6), 461–469.

U.S. Environmental Protection Agency (USEPA). (1996). "EPA liner study." *Rep. to Congress, Section 4113 (a) of the Pollution Act of 1990*, Washington, DC.

USEPA. (2005). "Secondary containment and impracticability determinations." Chapter 4, *Spill prevention, control, and countermeasure (SPCC) guidance for regional inspectors: Version 1.0*, Washington, DC.

van Genuchten, M. (1980). "A closed-form equation for predicting the hydraulic conductivity of unsaturated soils." *Soil Sci. Soc. Am. J.*, 44(5), 892–898.